C. R. Physique 17 (2016) 1084–1095

Contents lists available at ScienceDirect

Comptes Rendus Physique

www.sciencedirect.com

Mesoscopic thermoelectric phenomena / Phénomènes thermoélectriques mésoscopiques

Quantum-interference-enhanced thermoelectricity in single molecules and molecular films

Effets thermoélectriques amplifiés par interférences quantiques dans les molécules et les films moléculaires

Colin J. Lambert [a,*], Hatef Sadeghi [a], Qusiy H. Al-Galiby [a,b]

[a] *Department of Physics, Lancaster University, Lancaster LA1 4YB, UK*
[b] *Department of Physics, Education of College, Al Qadisiyah University, Iraq*

ARTICLE INFO

Article history:
Available online 18 August 2016

Keywords:
Molecular electronics
Thermoelectricity
Quantum interference
Seebeck coefficient

Mots-clés :
L'électronique moléculaire
Thermoélectricité
Interférence quantique
Coefficient Seebeck

ABSTRACT

We provide a brief overview of recent measurements and predictions of thermoelectric properties of single-molecules and porous nanoribbons and discuss some principles underpinning strategies for enhancing their thermoelectric performance. The latter include (a) taking advantage of steep slopes in the electron transmission coefficient $T(E)$, (b) creating structures with delta-function-like transmission coefficients and (c) utilising step-like features in $T(E)$. To achieve high performance, we suggest that the latter may be the most fruitful, since it is less susceptible to inhomogeneous broadening. For the purpose of extrapolating thermoelectric properties of single or few molecules to monolayer molecular films, we also discuss the relevance of the conductance-weighted average Seebeck coefficient.

RÉSUMÉ

Nous procédons à un bref survol des mesures et prédictions récentes concernant les propriétés thermoélectriques de molécules individuelles ou de nanorubans poreux, puis nous discutons quelques-uns des principes sous-jacents aux stratégies visant à augmenter leurs performances thermoélectriques. On relèvera parmi ces dernières (a) l'utilisation de pentes élevées du coefficient de transmission électronique $T(E)$, (b) la création de structures avec des pics de transmission et (c) l'exploitation de ces derniers. Pour atteindre de hautes performances, nous suggérons que cette dernière approche puisse être la plus fructueuse, puisqu'elle est moins susceptible de présenter des élargissements inhomogénes. Afin d'extrapoler les propriétés thermoélectriques d'une ou de quelques molécules à des films moléculaires monocouche, nous discutons aussi la pertinence de l'utilisation d'une moyenne du coefficient Seebeck pondérée par la conductance.

* Corresponding author.
E-mail addresses: c.lambert@lancaster.ac.uk (C.J. Lambert), h.sadeghi@lancaster.ac.uk (H. Sadeghi), q.agaliby@lancaster.ac.uk (Q.H. Al-Galiby).

http://dx.doi.org/10.1016/j.crhy.2016.08.003
1631-0705/

1. Introduction

Generation of electricity from waste heat via the Seebeck effect is silent, environmentally friendly and requires no moving parts. Waste heat from automobile exhausts, industrial manufacturing processes data farms and the human body could be used to generate electricity economically, provided more efficient thermoelectric materials could be realised. Conversely, Peltier cooling using high-performance thermoelectric materials would have applications ranging from on-chip cooling of CMOS-based devices to home refrigerators. This demand for new thermoelectric materials from the information technologies, aerospace, and automotive industries has led to a world-wide race to develop materials with a high thermoelectric efficiency, characterised by a high-dimensionless thermoelectric figure of merit $ZT = GS^2T/\kappa$, where G is the electrical conductance, S the Seebeck coefficient or thermopower, T the temperature, and κ the thermal conductance. In terms of ZT, the maximum efficiency of a thermoelectric generator is $\eta_{\max} = \eta_c(a-1)/(a+1)$, where η_c is the Carnot efficiency and $a = (ZT+1)^{1/2}$, whereas the efficiency at maximum power is $\eta_p = \eta_{CA}\ (a^2-1)/(a^2+1)$, where η_{CA} is the Curzon–Ahlborn upper bound. In both cases, the efficiency is at maximum when ZT tends to infinity. In most inorganic materials, the interdependency of transport coefficients constrains the options for materials design and makes optimisation a difficult task and, despite several decades of development, the best inorganic thermoelectric materials possess a figure of merit ZT slightly above unity only, which is not sufficient to create a viable technology platform for harvesting waste heat from data farms and the ambient environment. Generally, a compromise has been found in nanostructured semiconductors such as Bi_2Te_3 or PbTe–SrTe alloys. However, these materials are toxic and global supplies are limited. As an alternative, organic thermoelectric materials are now being investigated and are beginning to show promising values of both ZT and S. However, fundamental understanding at the molecular level is needed to increase these parameters to values beyond currently-attainable limits. During recent years, several groups have adopted a bottom–up approach to this challenge, by investigating thermoelectric properties of single molecules, which can be regarded as the ultimate nanostructured materials.

Current research in organic thermoelectrics aims to deliver high performance by exploiting room-temperature quantum interference (QI) at the single molecule level [1] and then translating this enhanced functionality to technologically-relevant thin-film materials and devices. Since thermopower is an intrinsic property, it should be possible to design molecules with built-in QI functionality and demonstrate that fundamental manifestations of QI can be manipulated and exploited in many-molecule ultra-thin films. Whereas single-molecules on gold or other metals can be electrically contacted using a STM tip, mono- or few-layer assemblies of molecules will require a planar top contact, which does not affect the integrity of the assembly [2]. For many years, this requirement has been a roadblock to the development of molecular-scale devices, because deposition of a top contact can easily degrade a molecular film. The use of graphene top contacts may overcome this roadblock [3–6] and allow the creation of a proper understanding of the integrity of the QI performance at the many-molecule level.

Although the dream of utilising quantum interference (QI) effects [6] in single molecules has been discussed for many years [7–14], experimental indications of room-temperature QI in single molecules were obtained only recently [15–22]. Building on these measurements, we anticipate the next breakthrough to be the active and continuous control of QI-based functionality in single-molecular junctions by external triggers, including electrostatic and mechanical gating. Indeed it has been demonstrated both experimentally and theoretically that at a molecular scale, thermopower S can be controlled by varying the chemical composition [23], tuning the position of intra-molecular energy levels relative to the work function of metallic electrodes [24,25], systematically increasing the single-molecule lengths and varying the binding groups within a family of molecules [26–30], by tuning the interaction between two neighbouring molecules [31], and by controlling the transport properties with an electrostatic [32] or electrochemical gate [33]. These single-molecule experiments yielded room-temperature values of S ranging in magnitude from ca. 1 to 50 μV/K. Furthermore mechanical gating of $Sc_3N@C_{80}$ [34] leads to bi-thermoelectric materials with S ranging from ±20 μV/K, depending on pressure and orientation.

Other approaches include developing strategies for increasing the thermopower of crown-ether-bridged anthraquinones [35]. The novel design feature of these molecules is the presence of either crown-ether or diaza-crown-ether bridges attached to the side of the current-carrying anthraquinone wire. The crown-ether side groups selectively bind alkali-metal cations, and when combined with TCNE or TTF dopants, provide a large phase-space for optimising thermoelectric properties. Recently, it was found [35] that the optimal combination of cations and dopants depends on the temperature range of interest. The thermopowers of both crown-ethers and diaza-crown-ethers are negative and at room temperature are optimised by binding with TTF alone, achieving thermopowers of −600 μV/K and −285 μV/K, respectively. At much lower temperatures, which are relevant to cascade coolers, crown ethers complexed with TTF and Na^+ are predicted to achieve a maximum thermopower of −710 μV/K at 70 K, whereas a combination of TTF and Li^+ yields a maximum thermopower of −600 μV/K at 90 K. For diaza-crown-ethers, it was found that TTF doping yields a maximum thermopower of −800 μV/K at 90 K, whereas at 50 K, the largest thermopower (of −600 μV/K) is obtained by a combination of TTF and K^+ doping. At room temperature, power factors of 73 μW/m·K^2 are predicted for crown-ether-bridged anthraquinones complexed with TTF and Na and 90 μW/m·K^2 for diaza crown-ether-bridged anthraquinones complexed with TTF. These compare favourably with power factors of other organic materials, whose reported values range from 0.016 μW/m·K^2 and 0.045 μW/m·K^2 for polyaniline and polypyrole respectively [36], to 12 μW/m·K^2 for PEDOT:PSS [46] and 12 μW/m·K^2 for C_{60}/Cs_2Co_3 Dph-BDT [47].

Recently [37], the thermoelectric properties of metalloporphyrins connected by thiol anchor groups to gold electrodes were investigated. By varying the transition-metal centre over the range Mn, Co, Ni, Cu, Fe, and Zn, their molecular en-

ergy levels can be tuned relative to the Fermi energy of the electrodes. The resulting single-molecule room-temperature thermopowers vary from almost zero for Co and Cu centres, to +80 μV/K and +230 μV/K for Ni and Zn, respectively. In contrast, the thermopowers with Mn(II) or Fe(II) metal centres are negative and lie in the range −280 to −260 μV/K. Complexing these with a counter anion to form Fe(III) and Mn(III) changes both the sign and magnitude of their thermopowers to +218 and +95 μV/K, respectively. These Seebeck coefficients are almost independent of temperature at room temperature and are significantly larger than recently-measured values of S at room temperature. For example, measured values include 8.7, 12.9 and 14.2 μV/K for 1,4-benzenedithiol (BDT), 4, 4′-dibenzenedithiol, and 4, 4″-tribenzenedithiol, respectively [38], −1.3 to 8.3 μV/K for the benzene-based series of benzene–dithiol (BDT), 2,5-dimethyl-1,4-benzenedithiol (BDT2Me), 2,3,5,6-tetrachloro-1,4-benzenedithiol (BDT4Cl), 2,3,5,6-tetraflouro-1,4-benzenedithiol (BDT4F) and BDCN [23,39], 7.7 to 15.9 μV/K for the series BDT, DBDT, TBDT and DMTBDT [40], −12.3 to 13.0 μV/K for a series of amine–Au and pyridine–Au linked molecules [41], and −8.9 to −33.1 μV/K for fullerene-based single-molecule junctions [24,41].

As noted in [1], organic thermoelectric materials may be an attractive alternative to inorganics for both thermoelectricity and thermal management, but at present the best organic thermoelectric material with a ZT of 0.6 at room temperature [42–45] is still not competitive with inorganics. Strategies for increasing $ZT = GS^2T/\kappa$ involve either increasing the numerator or decreasing the denominator. For comparison between single molecules and bulk materials, it is convenient to write $ZT = \frac{GS^2T}{\kappa} = \frac{\sigma_e S^2 T}{\gamma_T} = \frac{PT}{\gamma_T}$, where σ_e is the electrical conductivity, γ_T the thermal conductivity and $P = \gamma_e S^2$ the power factor. For a single molecule, the electrical conductivity is not well defined, but for the purpose of comparing with bulk materials, we define $\gamma_e = GL/A$, where L is the molecular length and A the area that the molecule would occupy in a SAM.

Strategies for reducing the denominator (i.e. κ) of ZT in single-molecule junctions are fundamentally different from those in inorganic bulk materials. In the latter, phonon transport can be reduced by nanostructuring [48,49], whereas molecular junctions are naturally nanostructured, and additional strategies based on molecular phonon conversion [50] become possible, including the reduction of thermal conductance due to weak overlap between the continuum of vibrational states in the electrodes and discrete vibrational states of the molecules or the weak interaction between different parts of the molecules, as in π–π stacked structures [51]. In the literature, there are many experiments addressing the vibrational properties of single molecules, but far fewer addressing single-molecule phonon transport, because it is extremely difficult to measure the thermal conductance of a single molecule. This difficulty is partly circumvented by scanning thermal microscope measurements of a few thousands of molecules in parallel, such as in a recent experimental study of the length-dependent thermal conductance of alkanes by the IBM group [52], which revealed a surprising initial increase in thermal conductance with length for short alkanes, due to interplay between the Debye frequency of the gold and that of the vibrational modes of the molecule [1]. This suggests that alternative metallic electrodes may be attractive [53,54]. Electroburnt graphene junctions are being developed for contacting single molecules [55–57,14,58,59], and form a new class of electrodes, which may be advantageous also in allowing reduction of the effects of defects in the electrodes [60] through the use of extended planar anchor groups [61–63]. Other strategies include introducing nanopores into two-dimensional nanoribbons formed from silicene or graphene [64,65], to reduce phonon transport and increase their Seebeck coefficients and figure of merit. As a first step in the development of strategies for maximising ZT, one often focuses on the so-called electronic figure of merit $ZT_e = \frac{GS^2T}{\kappa_e}$, where κ_e is the contribution from electron transport to the thermal conductance. Clearly, if κ_e vanishes, ZT_e can be infinite. However, for the purpose of maximising the full $ZT = \frac{GS^2T}{\kappa_e+\kappa_p}$, this is not too useful, because it means that the total thermal conductance $\kappa = \kappa_e + \kappa_p$ is dominated by the contribution from phonons, κ_p, and furthermore, if the Wiedemann–Franz law $\kappa_e \sim TG$ is satisfied, it means that the power factor vanishes. In what follows, we examine alternative strategies for optimising ZT.

2. Towards enhanced thermoelectricity in single molecules and molecular films

To understand how transport resonances and quantum interference lead to high thermoelectric performance, we note that in the linear-response regime, the electric current I and heat current $\dot{\mathbf{Q}}$ passing through a device is related to the voltage difference ΔV and temperature difference ΔT by [63]

$$\begin{pmatrix} I \\ \dot{Q} \end{pmatrix} = \frac{2}{h} \begin{pmatrix} e^2 L_0 & \frac{e}{T} L_1 \\ eL_1 & \frac{1}{T} L_2 \end{pmatrix} \begin{pmatrix} \Delta V \\ \Delta T \end{pmatrix} \tag{1}$$

where T is the reference temperature and

$$L_n = \int_{-\infty}^{\infty} (E - E_F)^n T(E) \left(-\frac{\partial f(E,T)}{\partial E} \right) \mathrm{d}E \tag{2}$$

In this expression, $e = -|e|$ is the electronic charge, $T(E)$ is the transmission coefficient for electrons of energy E, passing through the molecule from one electrode to the other and $f(E,T)$ is Fermi distribution defined as $f(E,T) = [\mathrm{e}^{(E-E_F)/k_BT} + 1]^{-1}$, where k_B is Boltzmann's constant.

When $\Delta T = 0$, Eq. (1) yields for the electrical conductance $G = (\frac{I}{\Delta V})_{\Delta T=0}$,

$$G = \frac{2e^2}{h} L_0 \tag{3}$$

Similarly when $I = 0$, Eq. (1) yields for the Seebeck coefficient $S = -(\frac{\Delta V}{\Delta T})_{I=0}$,

$$S = \frac{-1}{|e|T} \frac{L_1}{L_0} \tag{4}$$

Equation (1) can be rewritten in terms of the electrical conductance (G), thermopower (S), Peltier coefficient (Π), and the electronic contribution to the thermal conductance (κ_e):

$$\begin{pmatrix} \Delta V \\ \dot{Q} \end{pmatrix} = \begin{pmatrix} 1/G & S \\ \Pi & \kappa_e \end{pmatrix} \begin{pmatrix} I \\ \Delta T \end{pmatrix} \tag{5}$$

where

$$\Pi = \frac{-1}{|e|} \frac{L_1}{L_0} \tag{6}$$

$$\kappa_e = \frac{2}{hT} \left(L_2 - \frac{(L_1)^2}{L_0} \right) \tag{7}$$

From the above expressions, the electronic thermoelectric figure $ZT_e = S^2 GT/\kappa_e$ is given by

$$ZT_e = \frac{(L_1)^2}{L_0 L_2 - (L_1)^2} \tag{8}$$

3. Strategies for increasing thermoelectric performance

Based on the above expressions, we now examine three strategies for increasing thermoelectric performance.

3.1. Strategy 1: Utilising a steep slope in $T(E)$

For E close to E_F, if $T(E)$ varies approximately linearly with E on the scale of $k_B T$ then $L_0 \approx T(E_F)$, $L_1 \approx (eT)^2 \alpha (\frac{dT(E)}{dE})_{E=E_F}$ and $L_2 \approx (eT)^2 \alpha T(E_F)$, where α is the Lorenz number given by $\alpha = (\frac{1}{eT})^2 \int_{-\infty}^{\infty} (E - E_F)^2 (-\frac{\partial f(E,T)}{\partial E}) dE = (\frac{k_B}{e})^2 \frac{\pi^2}{3} = 2.44 \cdot 10^{-8}$ W·Ω·K^{-2}. Hence, in this limit, these formulae take the form [63]:

$$G \approx \left(\frac{2e^2}{h} \right) T(E_F) \tag{9}$$

$$S \approx -\alpha |e| T \left(\frac{d \ln T(E)}{dE} \right)_{E=E_F} \tag{10}$$

$$\kappa_e \approx \alpha T G \tag{11}$$

Equation (10) demonstrates that S is enhanced by increasing the slope of $\ln T(E)$, and hence quantum-interference-induced resonances or other features in $T(E)$ with steep slopes close to E_F are desirable. To estimate what constitutes a "steep slope", we note that the Wiedemann–Franz law, Eq. (11), yields:

$$ZT_e = \frac{S^2}{\alpha} \tag{12}$$

Therefore in the low-temperature limit, if $ZT_e > 1$, then we require $S^2 > \alpha$, i.e. $S > 150$ μV/K.

3.2. Strategy 2: Utilizing resonances in $T(E)$

Insight into alternative strategies for maximising ZT_e can be obtained by taking a 'statistical' view of Eqs. (3), (4), (7), and (8), which demonstrates why the denominator of Eq. (8) must be positive from a mathematical viewpoint. If the Fermi energy of the reservoirs is E_F, then it is convenient to introduce the non-normalised distribution $P(E) = -T(E) \frac{\partial f(E)}{\partial E}$ and the corresponding normalised distribution $\rho(E) = \frac{P(E)}{L_0}$. Then the mean of $(E - E_F)$ is $\langle E - E_F \rangle = \int dE \rho(E)(E - E_F)$ and the variance is $\sigma^2 = \langle (E - E_F)^2 \rangle - \langle E - E_F \rangle^2$. This yields for Eq. (4)

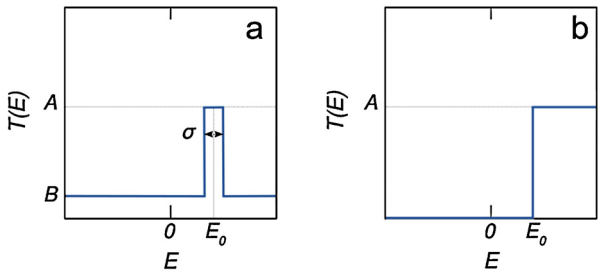

Fig. 1. Two ideal transmission coefficients T. (a) Delta-function like $T(E)$ and (b) Step-function like $T(E)$.

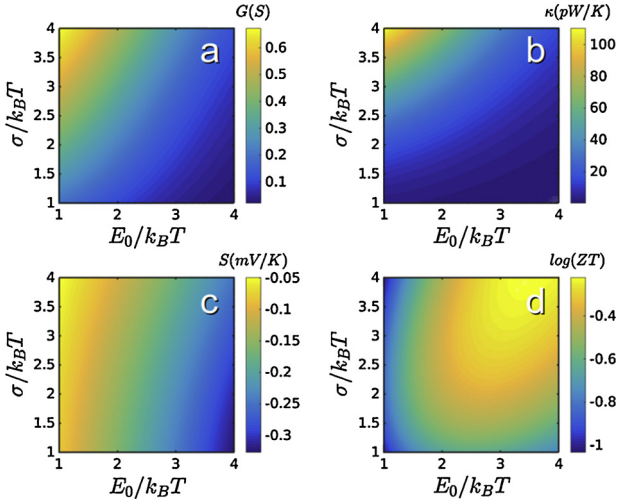

Fig. 2. Thermal properties of the delta-function-like $T(E)$, obtained with $E_F = 0$. (a) Conductance, (b) electronic thermal conductance, (c) thermopower and (d) total ZT by assuming a constant phonon thermal conductance. γ and σ are chosen to be 10.

$$S = \frac{-1}{|e|T}\langle E - E_F\rangle \tag{13}$$

Furthermore, Eq. (8) becomes

$$ZT_e = \frac{\langle E - E_F\rangle^2}{\sigma^2} \tag{14}$$

which is clearly positive.

The mean $\langle E - E_F\rangle$ and standard deviation σ capture essential features regarding the shape of $\rho(E)$ and $P(E)$. Equations (13) and (14) reveal that S and ZT_e depend only on these shape parameters and are independent of L_0. Only the electrical and electronic thermal conductances depend on L_0. This feature which can be traced to the fact that $G = \frac{2e^2}{h}L_0$ and $k_e = \frac{2L_0\sigma^2}{hT}$ describe the magnitudes of currents and therefore depend on the normalization L_0 of $P(E)$, whereas S and ZT_e involve only ratios. Clearly $\langle E - E_F\rangle$ will be non-zero only if $P(E) = -T(E)\frac{\partial f(E)}{\partial E}$ is an asymmetric function of $(E - E_F)$ and since $-\frac{\partial f(E)}{\partial E}$ is a symmetric function of $(E - E_F)$, $T(E)$ should be asymmetric with respect to E_F. Examples of two candidate transmission functions are shown in Fig. 1.

Fig. 1a is relevant for structures, whose electronic density of states contains narrow resonances, such as single-molecule electrical junctions. Equation (2) reveals that $ZT_e = \infty$, when $\sigma = 0$, which occurs when $T(E)$ is proportional to a delta function [64] of the form $T(E) = A\delta(E - E_0)$, in which case $\rho(E) = \delta(E - E_0)$, $S = \frac{-1}{|e|T}(E_0 - E_F)$ and ZT_e is infinite. Similarly $G = \frac{2e^2}{h}A(-\frac{\partial f(E_0)}{\partial E_0})$ and $k_e = 0$. The thermal properties of a system with a delta-function-like transmission are shown in Fig. 2.

Fig. 3 shows a physical realisation of a structure with delta-function-like transmission. In this case, the system consists of a silicene nanoribbon containing a nanopore and the delta function in $T(E)$ arises from the presence of edge states associated with zigzag edges of the ribbon [64].

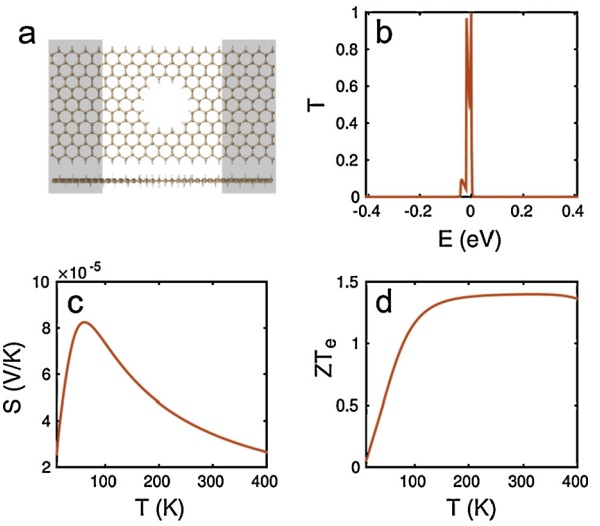

Fig. 3. (a) A silicene nanoribbon containing a nanopore with hydrogen terminated edges. (b) Transmission coefficient. (c) Thermopower. (d) Electronic ZT_e versus temperature. For convenience, $E_F = 0$.

3.3. Strategy 3: Utilising steps in $T(E)$

As alternative to using narrow transmission resonances, we now consider the step-like transmission shown in Fig. 1b, which occurs in periodic structures such as a crystalline nanoribbon or nanowire, where $T(E)$ is equal to the number of open channels and therefore changes in integer steps [65]. As a simple example, we now examine the thermopower and ZT_e of a system with a model step-like transmission coefficient of the form: $T(E) = A$ for $E > E_0$ and $T(E) = 0$ for $E < E_0$, where A is an arbitrary constant defining the height of the step and E_0 defines the position of the step. In this case, it is convenient to introduce the dimensionless parameter $y = (E - E_F)/k_BT$, so the Fermi function takes the form $f(E) = (\exp y + 1)^{-1}$, and write Eq. (2) in the form

$$L_n = A(k_BT)^n I_n(y_0) \tag{15}$$

where $y_0 = (E_0 - E_F)/k_BT$,

$$I_n(y_0) = \int_{y_0}^{\infty} \mathrm{d}y \left[-\frac{\mathrm{d}f}{\mathrm{d}y}\right] y^n \tag{16}$$

and $[-\frac{\mathrm{d}f}{\mathrm{d}y}] = \mathrm{e}^y/(\mathrm{e}^y + 1)^2$. Clearly, all moments depend only on the size of the step (i.e. the dimensionless parameter A) and the dimensionless parameter y_0, which defines the location of the step relative to the Fermi energy of the electrodes, in units of k_BT. In terms of I_n, $\langle E - E_F\rangle = k_BT\frac{I_1}{I_0}$, $\sigma^2 = (k_BT)^2[\frac{I_2}{I_0} - \frac{I_1^2}{I_0^2}]$. Plots of the dimensionless Fermi integrals $I_n(y_0)$ are shown in Fig. 4.

Clearly, $I_0(\infty) = 0$ and $I_0(-\infty) = 1$, because $I_0(y_0) = \int_{y_0}^{\infty} \mathrm{d}y[-\frac{\mathrm{d}f}{\mathrm{d}y}] = f(y_0) - f(\infty) = f(y_0)$. Also since $[-\frac{\mathrm{d}f}{\mathrm{d}y}]y$ is odd, $I_1(\mp\infty) = 0$ and $I_1(y_0)$ is a maximum at $y_0 = 0$. Furthermore, $I_2(-\infty) = \frac{\pi^2}{3}$ and since $[-\frac{\mathrm{d}f}{\mathrm{d}y}]y^2 = 0$ at $y = 0$, the slope of $I_2(y_0)$ vanishes at $y_0 = 0$.

In terms of $I_n(y_0)$, the thermoelectric parameters become

$$G = \frac{2e^2}{h} A I_0 \tag{17}$$

$$S = \frac{k_B}{e}\frac{I_1}{I_0} \tag{18}$$

$$k_e = \frac{2A(k_B)^2 T}{h}\left(I_2 - \frac{I_1^2}{I_0}\right) \tag{19}$$

$$ZT_e = \left[\frac{I_1^2}{I_0^2}\right] \Big/ \left[\frac{I_2}{I_0} - \frac{I_1^2}{I_0^2}\right] \tag{20}$$

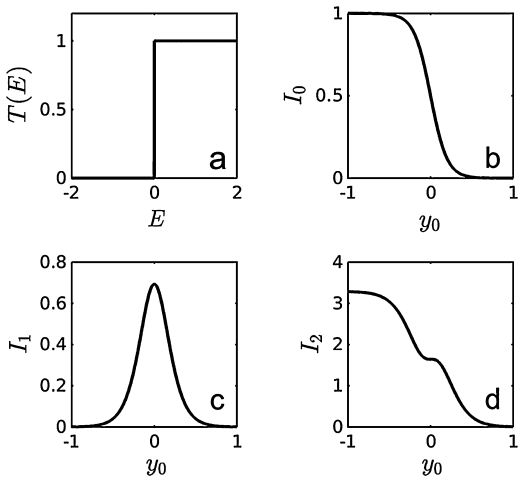

Fig. 4. I_0, I_1 and I_2 for a step-function like transmission coefficient.

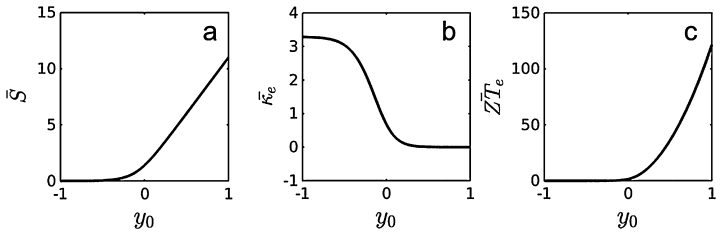

Fig. 5. Dimensionless thermopower $\bar{S}(y_0) = \frac{I_1}{I_0}$ and dimensionless electronic thermal conductance $\overline{k_e} = (I_2 - \frac{I_1^2}{I_0})$ and the electronic thermoelectric figure of merit ZT_e.

These equations show that the natural unit of G is $\frac{2e^2}{h} = 77$ μS, of S is $\frac{k_B}{e} = 86$ μV/K and of k_e is $\frac{2(k_B)^2 T}{h} = 173$ pW/K at room temperature (i.e. 300 K). Clearly, G and k_e are both proportional to step size A, whereas S and ZT_e are independent of A. Plots of the dimensionless thermopower $\bar{S} = \frac{I_1}{I_0}$ and dimensionless electronic thermal conductance $\overline{k_e} = (I_2 - \frac{I_1^2}{I_0})$ are shown in Fig. 5.

Obviously, since the moments L_n in Eq. (2) are linear in $T(E)$, the above analysis can be applied to various combinations of steps. For example, for the step-like transmission coefficient of the form: $T(E) = B$ for $E < E_0$ and $T(E) = 0$ for $E > E_0$, the relevant integrals are $J_n(y_0) = \int_{-\infty}^{y_0} \mathrm{d}y[-\frac{\mathrm{d}f}{\mathrm{d}y}]y^n$ and Eq. (15) is replaced by $L_n = B(k_B T)^n J_n(y_0)$ (Fig. 6).

Similarly, for a two-step transmission of the form $T(E) = B$ for $E < E_0$ and $T(E) = 0$ for $E_1 > E > E_0$ and $T(E) = B$ for $E > E_1$, $L_n = (k_B T)^n [B J_n(y_1) + A I_n(y_0)]$, etc.

So far we have ignored phonons, whose contribution to the thermal conductance is

$$\kappa_{\mathrm{ph}}(T) = \frac{1}{2\pi} \int_0^\infty \hbar\omega T_{\mathrm{ph}}(\omega) \frac{\partial f_{\mathrm{BE}}(\omega, T)}{\partial T} \mathrm{d}\omega \tag{21}$$

where $f_{\mathrm{BE}}(\omega, T) = (\mathrm{e}^{\hbar\omega/k_B T} - 1)^{-1}$ is the Bose–Einstein distribution function and $T_{\mathrm{ph}}(\omega)$ is the transmission coefficient for phonons of energy $\hbar\omega$ [1]. Since

$$\frac{\partial f_{\mathrm{BE}}(\omega, T)}{\partial T} = \left[\hbar\omega/k_B T^2\right] \mathrm{e}^{\hbar\omega/k_B T} \left(\mathrm{e}^{\hbar\omega/k_B T} - 1\right)^{-2} \tag{22}$$

$$\kappa_{\mathrm{ph}}(T) = \frac{k_B}{2\pi} \int_0^\infty T_{\mathrm{ph}}(\omega) [\hbar\omega/k_B T]^2 \mathrm{e}^{\hbar\omega/k_B T} \left(\mathrm{e}^{\hbar\omega/k_B T} - 1\right)^{-2} \mathrm{d}\omega \tag{23}$$

$$\kappa_{\mathrm{ph}}(T) = \frac{3g_0}{\pi^2} \int_0^\infty T_{\mathrm{ph}}(y) y^2 \mathrm{e}^y \left(\mathrm{e}^y - 1\right)^{-2} \mathrm{d}y \tag{24}$$

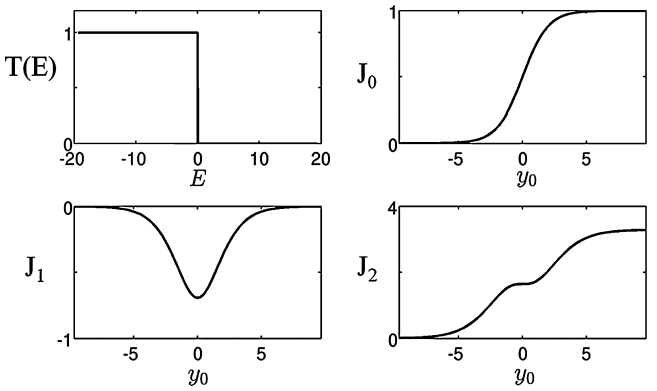

Fig. 6. J_0, J_1 and J_2 for a step-function-like transmission coefficient. (These can be obtained from Fig. 4 by symmetry.)

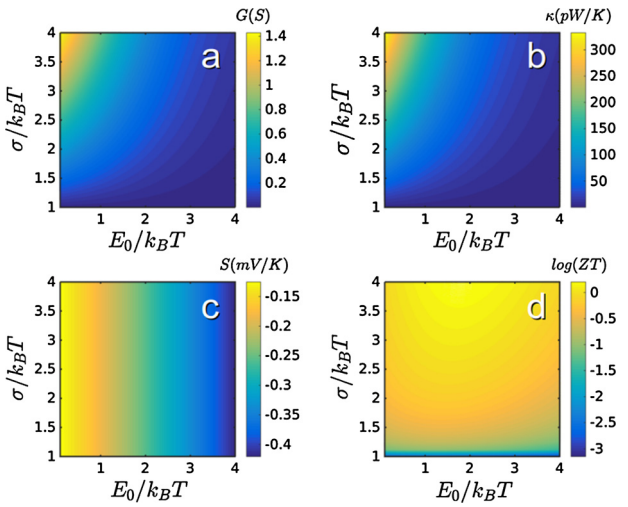

Fig. 7. Thermal properties of the step-function like $T(E)$. (a) Conductance. (b) Electronic thermal conductance. (c) Thermopower. (d) Total ZT by assuming a constant phonon thermal conductance 300 pW/K. γ and σ are chosen to be 10.

In this expression, the quantum of thermal conductance is $g_0 = \frac{(\frac{\pi}{6})(k_B)^2}{\hbar} T = (9.456 \cdot 10^{-13}\ \mathrm{W/K^2})T$. As an example, the quantum of thermal conductance g_0 is 284 pW/K, at room temperature, which is the maximum room-temperature phonon thermal conductance per channel and occurs only if the upper cut off of the phonon channel is greater than approximately $5k_BT$. In contrast, for electrons, the quantum of phonon thermal conductance is $\frac{2(k_B)^2T}{h} = \frac{(k_B)^2T}{\pi\hbar} = 173$ pW/K at room temperature.

For the above step-like model of electron transmission, where $T(E) = A$ for $E > E_0$ and $T(E) = 0$ for $E < E_0$, two-dimensional plots of thermoelectric coefficients are shown in Fig. 7, where when computing the full ZT, we have assumed a phonon thermal conductance of $\kappa_p = 300$ pW/K.

Fig. 8 shows an example of a graphene nanoribbon with step-function-like electron transmission coefficient around the Fermi energy $E_F = 0$ [65]. The structure is formed by two overlapping monolayer ribbons with hydrogen edge terminations, with the overlapping bilayer region containing a nanopore, whose edges are terminated by oxygen. Electrons flow from a left electrode connected to the top ribbon, to an electrode connected to the bottom ribbon, through the overlap region. Over the energy interval shown, there is one open scattering channel in the crystalline nanoribbons. In this case, the oxygen-terminated pore blocks electron transmission over the energy interval 0 to 0.2 eV, and an asymmetric step in $T(E)$ arises from the asymmetry created by the presence of the oxygens.

3.4. Strategy 4: Minimizing the effect of inhomogeneous broadening

In a thin film, such as that shown in Fig. 9, the properties of many molecules in parallel will depend on intermolecular interactions, quantum interference between nearby molecules mediated by the contacts, defects in the electrodes, impurities, pinholes, and fluctuations in dopant concentrations.

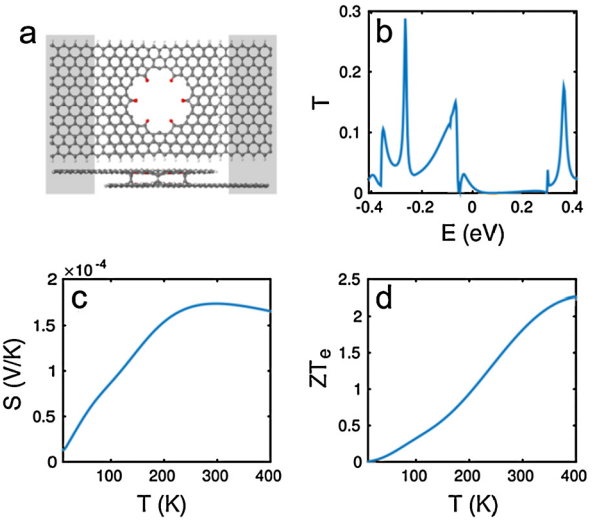

Fig. 8. (a) Bilayer graphene nanoribbon with hydrogen terminated edges and containing a nanopore whose inner edge is oxygen terminated. (a) Molecular structure. (b) Transmission coefficient. (c) Thermopower. (d) Electronic ZT_e at $E_F = 0$ and versus temperature.

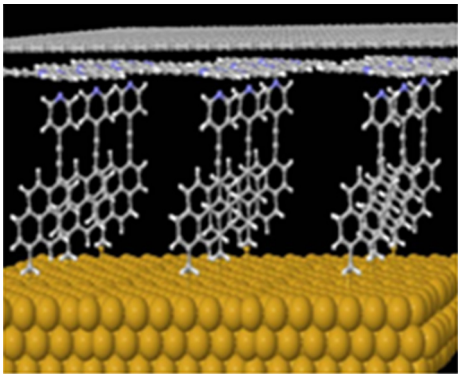

Fig. 9. A SAM formed on a gold bottom electrode, in contact with a graphene top electrode.

As a first step towards understanding the role of such inhomogeneous broadening, if intermolecular interactions are ignored in a SAM of N molecules in parallel, then if molecule j has a transmission coefficient $T_j(E)$, the moments L_n appearing in Eqs. (1), and all subsequent equations should be replaced by $\overline{L}_n = \sum_{j=1}^{N} L_n^j$, where

$$L_n^j = \int_{-\infty}^{\infty} (E - E_F)^n T_j(E) \left(-\frac{\partial f(E,T)}{\partial E} \right) dE \tag{25}$$

This means that Eq. (4) is replaced by

$$S = \frac{-1}{|e|T} \frac{\overline{L}_1}{\overline{L}_0} = \frac{\overline{SG}}{\overline{G}} \tag{26}$$

The conductance-weighted averaged Seebeck coefficient $S = \frac{\overline{SG}}{\overline{G}}$ is quite different from the average $\tilde{S} = (\frac{1}{N}) \sum_{j=1}^{N} S_j$, where $S_j = \frac{-1}{|e|T} \frac{L_1^j}{L_0^j}$ is the Seebeck coefficient of molecule j. Indeed $\tilde{S}$ is dominated by large individual values of S_j (i.e. molecules with small values of electrical conductance L_0^j), whereas small values of G do not contribute significantly to $\overline{SG}$. Since $\overline{L}_n = \int_{-\infty}^{\infty} (E - E_F)^n \overline{T}(E) (-\frac{\partial f(E,T)}{\partial E}) dE$, where $\overline{T}(E) = \sum_{j=1}^{N} T_j(E)$, then the advantages of steep slopes or sharp delta-function like resonances in $T_j(E)$ will be lost if such features appear at different random energies for different molecules. This suggests that as a strategy for optimising thermoelectric performance, the delta-function-like transmission of Fig. 1a has drawbacks, because the sign of the thermopower and the coefficients L_1^j depend on the location of the resonance E_0. This

means that due to inhomogeneous broadening, the thermopower of a self-assembled monolayer of such molecules may be very low, even though the thermopower of each individual molecule is high. Furthermore, since the electronic thermal conductance vanishes, the denominator of the full figure of merit is dominated by phonons, so the fact that $ZT_e = \infty$, when the width of the resonance vanishes is irrelevant. On the other hand, as shown in Figs. 4c and 5a, fluctuations in the positions of step-like features in $T(E)$ do not change the sign of the Seebeck coefficient and therefore molecules or nanoribbons exhibiting step-like transmission coefficients may be more resilient to inhomogeneous broadening.

The above classical behaviour occurs when the spacing between molecules is greater than the inelastic scattering length (sometimes called the dephasing length) l_φ, beyond which a classical Boltzmann-based description can be used. In a denser SAM, the role of intermolecular interactions would have to be included up to length scales of order l_φ. In this case, one should divide the SAM into M plaquettes of area l_φ^2 and compute the coefficients $L_0^{(A)}$ and $L_1^{(A)}$ for each plaquette (labelled A), whose values will depend on the arrangement of the $\frac{N}{M}$ molecules within each plaquette and on defects in the electrodes contacting the plaquette. The quantities $\overline{L_n}$ would then be averages over all such plaquettes; i.e. $\overline{L_n} = \frac{1}{M}\sum_A L_n^{(A)}$. In this expression, $L_n^{(A)}$ is not simply an average over single-molecule values $L_n^{(a)}$, but instead should be computed by solving for the transmission coefficient of a whole plaquette or measured in for example an STM break junction using a tip of cross sectional area greater than or equal to l_φ^2. Nevertheless, with this redefinition of $\overline{L_n}$, Eqs. (25) and (26) remain unchanged.

4. Conclusion

In conclusion, we have provided a brief overview of recent measurements and predictions of thermoelectric properties of single-molecule and nanoribbons and discussed some principles underpinning strategies for enhancing their thermoelectric performance. The latter include (a) taking advantage of steep slopes in $T(E)$, (b) creating structures with delta-function-like transmission coefficients and (c) utilising step-like features in $T(E)$. To achieve high performance, these strategies should be combined with methods for reducing inhomogeneous broadening and minimising the phonon thermal conductance. Of the above three strategies, the third one appears to be the most resilient. It is not yet known if these strategies will be successful in achieving values of ZT in excess of unity in organic thin films. However, for structures obeying the Wiedemann–Franz law, this is possible, provided the Seebeck coefficient exceeds $S = 150\ \mu V/K$. Diaza-crown-ethers and metallo-porphyrins are predicted to possess Seebeck coefficients exceeding this value and therefore there are grounds for optimism.

Acknowledgements

This work was supported by the European Commission (EC) FP7 ITN “MOLESCO” (project No. 606728) and UK EPSRC (Grant Nos. EP/M014452/1 and EP/N017188/1).

References

[1] H. Sadeghi, S. Sangtarash, C.J. Lambert, Oligoyne molecular junctions for efficient room temperature thermoelectric power generation, Nano Lett. 15 (11) (2015) 7467–7472.
[2] G.J. Ashwell, B. Urasinska, C. Wang, M.R. Bryce, I. Grace, C.J. Lambert, Single-molecule electrical studies on a 7 nm long molecular wire, Chem. Commun. 45 (2006) 4706–4708.
[3] H. Akkerman, P. Blom, D. De Leeuw, B. De Boer, Towards molecular electronics with large-area molecular junctions, Nature 441 (7089) (2006) 69–72.
[4] T. Li, J. Hauptmann, Z. Wei, Solution processed ultrathin chemically derived graphene films as soft top contacts for solid state molecular electronic junctions, Adv. Mater. 24 (10) (2012) 1333–1339.
[5] G. Wang, Y. Kim, M. Choe, T.-W. Kim, T. Lee, A new approach for molecular electronic junctions with a multilayer graphene electrode, Adv. Mater. 23 (6) (2011) 755–760.
[6] A. Neuhausen, A. Hosseini, J.A. Sulpizio, C.E.D. Chidsey, D. Goldhaber-Gordon, Molecular junctions of self-assembled monolayers with conducting polymer contacts, ACS Nano 6 (11) (2012) 9920–9931.
[7] M. Magoga, C. Joachim, Conductance of molecular wires connected or bonded in parallel, Phys. Rev. B 59 (24) (1999) 16011–16021.
[8] C.M. Finch, V.M. García-Suárez, C.J. Lambert, Giant thermopower and figure of merit in single-molecule devices, Phys. Rev. B, Condens. Matter Mater. Phys. 79 (2009) 2–5.
[9] J.P. Bergfield, C.A. Stafford, Thermoelectric signatures of coherent transport in single-molecule heterojunctions, Nano Lett. 9 (8) (2009) 3072–3076.
[10] M. Bürkle, L. Zotti, J. Viljas, D. Vonlanthen, A. Mishchenko, T. Wandlowski, M. Mayor, G. Schön, F. Pauly, *Ab initio* study of the thermopower of biphenyl-based single-molecule junctions, Phys. Rev. B 86 (11) (2012) 115304.
[11] O. Entin-Wohlman, Y. Imry, A. Aharony, Three-terminal thermoelectric transport through a molecular junction, Phys. Rev. B 82 (11) (2010) 115314.
[12] S. Sangtarash, C. Huang, H. Sadeghi, G. Sorohhov, J. Hauser, T. Wandlowski, W. Hong, S. Decurtins, S.-X. Liu, C.J. Lambert, Searching the hearts of graphene-like molecules for simplicity, sensitivity, and logic, J. Am. Chem. Soc. 137 (35) (2015) 11425–11431.
[13] Y. Geng, S. Sangtarash, C. Huang, H. Sadeghi, Y. Fu, W. Hong, T. Wandlowski, S. Decurtins, C.J. Lambert, S.-X. Liu, Magic ratios for connectivity-driven electrical conductance of graphene-like molecules, J. Am. Chem. Soc. 137 (13) (2015) 4469–4476.
[14] H. Sadeghi, J.A. Mol, C.S. Lau, G.A.D. Briggs, J. Warner, C.J. Lambert, Conductance enlargement in picoscale electroburnt graphene nanojunctions, Proc. Natl. Acad. Sci. USA 112 (9) (2015) 2658–2663.
[15] H. Vazquez, R. Skouta, S. Schneebeli, M. Kamenetska, R. Breslow, L. Venkataraman, M.S. Hybertsen, Probing the conductance superposition law in single-molecule circuits with parallel paths, Nat. Nanotechnol. 7 (10) (2012) 663–667.
[16] S. Ballmann, R. Härtle, P.B. Coto, M. Elbing, M. Mayor, M.R. Bryce, M. Thoss, H.B. Weber, Experimental evidence for quantum interference and vibrationally induced decoherence in single-molecule junctions, Phys. Rev. Lett. 109 (5) (2012) 1–5.
[17] S.V. Aradhya, J.S. Meisner, M. Krikorian, S. Ahn, R. Parameswaran, M.L. Steigerwald, C. Nuckolls, L. Venkataraman, Dissecting contact mechanics from quantum interference in single-molecule junctions of stilbene derivatives, Nano Lett. 12 (3) (2012) 1643–1647.

[18] V. Kaliginedi, P. Moreno-García, H. Valkenier, W. Hong, V.M. García-Suárez, P. Buiter, J.L.H. Otten, J.C. Hummelen, C.J. Lambert, T. Wandlowski, Correlations between molecular structure and single-junction conductance: a case study with oligo(phenylene–ethynylene)-type wires, J. Am. Chem. Soc. 134 (11) (2012) 5262–5275.
[19] S.V. Aradhya, L. Venkataraman, Single-molecule junctions beyond electronic transport, Nat. Nanotechnol. 8 (6) (2013) 399–410.
[20] C.R. Arroyo, S. Tarkuc, R. Frisenda, J.S. Seldenthuis, C.H.M. Woerde, R. Eelkema, F.C. Grozema, H.S.J. van der Zant, Signatures of quantum interference effects on charge transport through a single benzene ring, Angew. Chem., Int. Ed. Engl. 52 (11) (2013) 3152–3155.
[21] C.M. Guédon, H. Valkenier, T. Markussen, K.S. Thygesen, J.C. Hummelen, S.J. van der Molen, Observation of quantum interference in molecular charge transport, Nat. Nanotechnol. 7 (5) (2012) 305–309.
[22] F. Prins, A. Barreiro, J.W. Ruitenberg, J.S. Seldenthuis, N. Aliaga-Alcalde, L.M.K. Vandersypen, H.S.J. van der Zant, Room-temperature gating of molecular junctions using few-layer graphene nanogap electrodes, Nano Lett. 11 (11) (2011) 4607–4611.
[23] K. Baheti, J.A. Malen, P. Doak, P. Reddy, S.Y. Jang, T.D. Tilley, A. Majumdar, R.A. Segalman, Probing the chemistry of molecular heterojunctions using thermoelectricity, Nano Lett. 8 (2) (2008) 715–719.
[24] S.K. Yee, J.A. Malen, A. Majumdar, R.A. Segalman, Thermoelectricity in fullerene–metal heterojunctions, Nano Lett. 11 (10) (2011) 4089–4094.
[25] S.K. Lee, T. Ohto, R. Yamada, H. Tada, Thermopower of benzenedithiol and C_{60} molecular junctions with Ni and Au electrodes, Nano Lett. 14 (9) (2014) 5276–5280.
[26] J. Malen, P. Doak, K. Baheti, Identifying the length dependence of orbital alignment and contact coupling in molecular heterojunctions, Nano Lett. 9 (3) (2009) 1164–1169.
[27] A. Tan, J. Balachandran, S. Sadat, V. Gavini, B.D. Dunietz, S.-Y. Jang, P. Reddy, Effect of length and contact chemistry on the electronic structure and thermoelectric properties of molecular junctions, J. Am. Chem. Soc. 133 (23) (2011) 8838–8841.
[28] J. Balachandran, P. Reddy, End-group-induced charge transfer in molecular junctions: effect on electronic-structure and thermopower, J. Phys. Chem. Lett. 3 (15) (2012) 1962–1967.
[29] J.R. Widawsky, W. Chen, H. Vázquez, T. Kim, R. Breslow, M.S. Hybertsen, L. Venkataraman, Length-dependent thermopower of highly conducting Au–C bonded single molecule junctions, Nano Lett. 13 (6) (2013) 2889–2894.
[30] W.B. Chang, C. Mai, M. Kotiuga, J.B. Neaton, G.C. Bazan, R.A. Segalman, Controlling the thermoelectric properties of thiophene-derived single-molecule junctions, Chem. Mater. 26 (24) (2014) 7229–7235.
[31] C. Evangeli, K. Gillemot, E. Leary, M.T. González, G. Rubio-Bollinger, C.J. Lambert, N. Agraït, Engineering the thermopower of C_{60} molecular junctions, Nano Lett. 13 (5) (2013) 2141–2145.
[32] Y. Kim, W. Jeong, K. Kim, W. Lee, P. Reddy, Electrostatic control of thermoelectricity in molecular junctions, Nat. Nanotechnol. 9 (11) (2014) 881–885.
[33] V.M. García-Suárez, C.J. Lambert, D. Zs Manrique, T. Wandlowski, Redox control of thermopower and figure of merit in phase-coherent molecular wires, Nanotechnology 25 (2014) 205402.
[34] L. Rincón-García, A.K. Ismael, C. Evangeli, I. Grace, G. Rubio-Bollinger, K. Porfyrakis, N. Agraït, C.J. Lambert, Molecular design and control of fullerene-based bi-thermoelectric materials, Nat. Mater. 15 (3) (2016) 289–293.
[35] A. Ismael, I. Grace, C. Lambert, Increasing the thermopower of crown-ether-bridged anthraquinones, Nanoscale 7 (41) (2015) 17338–17342.
[36] A. Shakouri, Thermoelectric power factor for electrically conductive polymers, in: Proc. Eighteenth Int. Conf. Thermoelectr., ICT'99, 1999, pp. 402–406 (Cat. No. 99TH8407) (c).
[37] Q. Al-Galiby, H. Sadeghi, L. Algharagholy, Tuning the thermoelectric properties of metallo-porphyrins, Nanoscale 8 (4) (2016) 2428–2433.
[38] P. Reddy, S.-Y. Jang, R.A. Segalman, A. Majumdar, Thermoelectricity in molecular junctions, Science 315 (5818) (2007) 1568–1571.
[39] J.A. Malen, S.K. Yee, A. Majumdar, R.A. Segalman, Fundamentals of energy transport, energy conversion, and thermal properties in organic–inorganic heterojunctions, Chem. Phys. Lett. 491 (4–6) (2010) 109–122.
[40] J.A. Malen, P. Doak, K. Baheti, T.D. Tilley, A. Majumdar, R.A. Segalman, The nature of transport variations in molecular heterojunction electronics, Nano Lett. 9 (10) (2009) 3406–3412.
[41] J.R. Widawsky, P. Darancet, J.B. Neaton, L. Venkataraman, Simultaneous determination of conductance and thermopower of single molecule junctions, Nano Lett. 12 (1) (2012) 354–358.
[42] D. Chung, CsBi4Te6: a high-performance thermoelectric material for low-temperature applications, Science 287 (5455) (2000) 1024–1027.
[43] L.-D. Zhao, V.P. Dravid, M.G. Kanatzidis, The panoscopic approach to high performance thermoelectrics, Energy Environ. Sci. 7 (1) (2014) 251–268.
[44] Q. Zhang, Y. Sun, W. Xu, D. Zhu, Organic thermoelectric materials: emerging green energy materials converting heat to electricity directly and efficiently, Adv. Mater. 26 (40) (2014) 6829–6851.
[45] S. Majumdar, J.A. Sierra-Suarez, S.N. Schiffres, W.-L. Ong, C.F. Higgs, A.J.H. McGaughey, J.A. Malen, Vibrational mismatch of metal leads controls thermal conductance of self-assembled monolayer junctions, Nano Lett. 15 (5) (2015) 2985–2991.
[46] H. Shi, C. Liu, J. Xu, H. Song, Electrochemical fabrication and thermoelectric performance of the PEDOT: PSS electrode based bilayered organic nanofilms, Int. J. Electrochem. Sci. 9 (2014) 7629–7643.
[47] M. Sumino, K. Harada, M. Ikeda, S. Tanaka, K. Miyazaki, C. Adachi, Thermoelectric properties of *n*-type C_{60} thin films and their application in organic thermovoltaic devices, Appl. Phys. Lett. 99 (9) (2011) 093308.
[48] G. Fagas, A.G. Kozorezov, C.J. Lambert, J.K. Wigmore, A. Peacock, A. Poelaert, R. den Hartog, Lattice dynamics of a disordered solid–solid interface, Phys. Rev. B 60 (9) (1999) 6459–6464.
[49] A. Kambili, G. Fagas, V.I. Fal'ko, C.J. Lambert, Phonon-mediated thermal conductance of mesoscopic wires with rough edges, Phys. Rev. B 60 (23) (1999) 15593–15596.
[50] R.Y. Wang, R.A. Segalman, A. Majumdar, Room temperature thermal conductance of alkanedithiol self-assembled monolayers, Appl. Phys. Lett. 89 (17) (2006) 173113.
[51] G. Kiršanskas, Q. Li, K. Flensberg, G.C. Solomon, M. Leijnse, Designing π-stacked molecular structures to control heat transport through molecular junctions, Appl. Phys. Lett. 105 (23) (2014) 233102.
[52] T. Meier, F. Menges, P. Nirmalraj, H. Hölscher, H. Riel, B. Gotsmann, Length-dependent thermal transport along molecular chains, Phys. Rev. Lett. 113 (6) (2014) 060801.
[53] V. García-Suárez, A. Rocha, S. Bailey, Single-channel conductance of H_2 molecules attached to platinum or palladium electrodes, Phys. Rev. B 72 (2005) 045437.
[54] V. García-Suárez, Optimized basis sets for the collinear and non-collinear phases of iron, J. Phys. Condens. Matter 16 (30) (2004) 5453.
[55] E. Burzurí, Characterization of nanometer-spaced few-layer graphene electrodes, Graphene 01 (02) (2012) 26–29.
[56] A. Barreiro, F. Börrnert, M.H. Rümmeli, B. Büchner, L.M.K. Vandersypen, Graphene at high bias: cracking, layer by layer sublimation, and fusing, Nano Lett. 12 (4) (2012) 1873–1878.
[57] Y. Lu, C.A. Merchant, M. Drndić, A.T.C. Johnson, *In situ* electronic characterization of graphene nanoconstrictions fabricated in a transmission electron microscope, Nano Lett. 11 (12) (2011) 5184–5188.
[58] H. Sadeghi, S. Sangtarash, C. Lambert, Hexagonal-boron nitride substrates for electroburnt graphene nanojunctions, Physica E, Low-Dimens. Syst. Nanostruct. 82 (2016) 12–15, http://dx.doi.org/10.1016/j.physe.2015.09.005.
[59] H. Sadeghi, S. Sangtarash, C.J. Lambert, Electron and heat transport in porphyrin-based single-molecule transistors with electro-burnt graphene electrodes, Beilstein J. Nanotechnol. 2015 (6) (2015) 1413–1420.

[60] C.J. Lambert, D.L. Weaire, Theory of the arrangement of cells in a network, Metallography 14 (4) (1981) 307–318.
[61] S. Bailey, D. Visontai, C.J. Lambert, M.R. Bryce, H. Frampton, D. Chappell, A study of planar anchor groups for graphene-based single-molecule electronics, J. Chem. Phys. 140 (5) (2014) 054708.
[62] C.G. Péterfalvi, C.J. Lambert, Suppression of single-molecule conductance fluctuations using extended anchor groups on graphene and carbon-nanotube electrodes, Phys. Rev. B 86 (8) (2012) 085443.
[63] C.J. Lambert, Basic concepts of quantum interference and electron transport in single-molecule electronics, Chem. Soc. Rev. 44 (4) (2015) 875–888.
[64] H. Sadeghi, S. Sangtarash, C.J. Lambert, Enhanced thermoelectric efficiency of porous silicene nanoribbons, Sci. Rep. 5 (2015) 9514.
[65] H. Sadeghi, S. Sangtarash, C.J. Lambert, Enhancing the thermoelectric figure of merit in engineered graphene nanoribbons, Beilstein J. Nanotechnol. 6 (1) (2015) 1176–1182.